Journal of Materials Chemistry A

COMMUNICATION

View Article Online
View Journal | View Issue

Cite this: J. Mater. Chem. A, 2015, 3, 6286

Received 1st January 2015
Accepted 19th February 2015

DOI: 10.1039/c5ta00007f

www.rsc.org/MaterialsA

A redox-active gel electrolyte for fiber-shaped supercapacitor with high area specific capacitance†

Shaowu Pan,[ab] Jue Deng,[b] Guozhen Guan,[b] Ye Zhang,[b] Peining Chen,[b] Jing Ren[b] and Huisheng Peng*[ab]

A new redox-active gel electrolyte has been developed by adding 2-mercaptopyridine to poly(vinyl alcohol)–H_2SO_4 and exhibits reversible redox reactions for a high pseudocapacitance. Upon combination with carbon nanotube/mesoporous carbon hybrid fibers that show large surface areas to fabricate a fiber-shaped supercapacitor, an area specific capacitance of 507.02 mF cm^{-2} has been achieved.

Introduction

Wearable fiber-shaped supercapacitors (FSSs)[1–5] have attracted increasing interests due to the combined advantages of small size, light weight and high flexibility. However, the relatively low electrochemical performance of the FSSs has severely limited their practical applications. To this end, a lot of efforts are made to enhance their electrochemical properties by introducing new materials[6–13] and optimizing device structures.[14–17] Typically, electrochemically active metal oxides[18–22] and conductive polymers[23–25] are deposited into the fiber electrode for high specific capacitances. For instance, a FSS based on bare carbon nanotube (CNT) fibers exhibited an area specific capacitance of 1.97 mF cm^{-2}.[13] After incorporation of MnO_2, Co_3O_4/NiO, polyaniline and poly(3,4-ethylenedioxythiophene), the area specific capacitances are increased to *e.g.*, 3.71,[21] 52.6,[22] 38 (ref. 24) and 73 mF cm^{-2},[25] respectively. The optimization of the fiber electrode has been discovered as another general and promising method in enhancing the specific capacitance. For instance, a graphene/CNT core–sheath fiber is designed and used to offer a high area specific capacitance of 177 mF cm^{-2}.[12] Although the specific capacitances of FSSs have been greatly improved in the past years, they are still far away from the expected levels by practical applications.

In this Communication, we present a new and general strategy to produce the FSS with much increased area specific capacitance through the use of an effective redox-active gel electrolyte that is prepared by adding 2-mercaptopyridine (PySH), an electrochemical active compound, to the PVA–H_2SO_4 electrolyte. For the resulting FSS based on two aligned CNT/mesoporous carbon (MC) hybrid fiber electrodes, a high specific capacitance of 507.02 mF cm^{-2} (or 17.51 mF cm^{-1}) has been achieved and well maintained after 1000 cycles. This FSS is also flexible, and the specific capacitance can retain by above 97% after bending for 500 cycles.

Experimental section

Preparation of the PVA–H_2SO_4–PySH gel electrolyte

Polyvinyl alcohol (1 g) was added to deionized water (10 g) and swelled for 4 h at room temperature, followed by heating at 95 °C under vigorous stirring for 1.5 h. H_2SO_4 (0.01 mol) and 2-mercaptopyridine (0–0.3 g) were then added to the above solution to obtain a homogeneous gel under stirring.

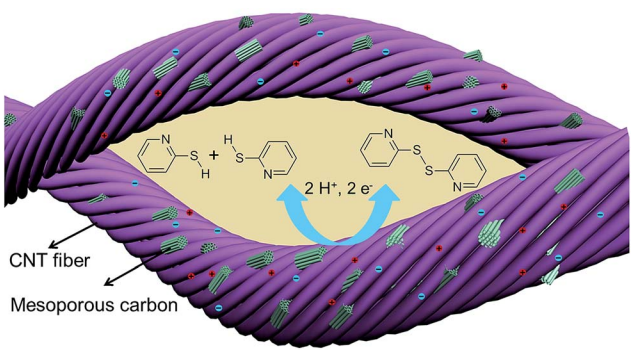

Fig. 1 Schematic illustration to the working mechanism of a FSS based on the redox-active gel electrolyte.

[a]School of Materials Science and Engineering, Institute for Advanced Materials and Nano Biomedicine, Tongji University, 4800 Caoan Road, Shanghai 201804, China
[b]State Key Laboratory of Molecular Engineering of Polymers, Department of Macromolecular Science and Laboratory of Advanced Materials, Fudan University, Shanghai 200438, China. E-mail: penghs@fudan.edu.cn

† Electronic supplementary information (ESI) available. See DOI: 10.1039/c5ta00007f

Fabrication of FSSs

CNT sheets were prepared from spinnable CNT arrays,[26] and three layers of CNT sheets with the same width of 1.5 cm were stacked together along the length direction, followed by addition of an MC (provided by XF Nano, INC Advanced Material Supplier, pore diameter: 3–5 nm) dispersion in *N*,*N*-dimethylformamide. The CNT/MC hybrid fibers with different MC weight percentages were prepared using solutions with different MC concentrations (0.1, 0.4, 0.7 and 1.0 mg mL^{-1}). The resulting CNT and MC hybrid sheet was rolled into a fiber at a rotary rate of 1000 rpm. After drying in a vacuum for 24 h, the hybrid fiber was coated with a layer of the gel electrolyte which also served as the separator and dried at room temperature. Two hybrid fibers were twisted together, followed by coating of the gel electrolyte again to produce a FSS.

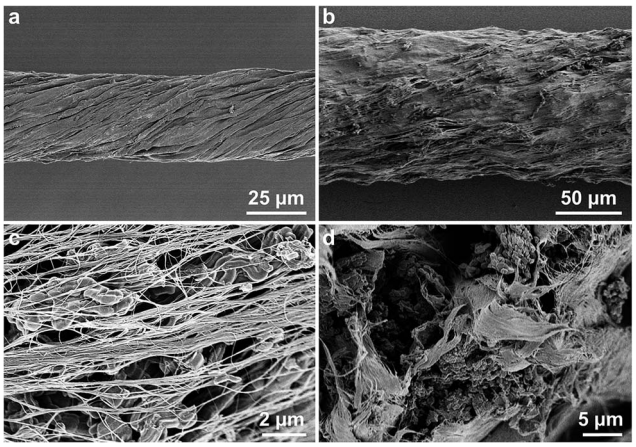

Fig. 2 SEM images of the aligned CNT fiber before and after incorporation of MC. (a) A bare CNT fiber. (b and c) A CNT/MC hybrid fiber (MC weight percentage of 68%) at low and high magnifications, respectively. (d) Cross-sectional image of the CNT/MC fiber.

Results and discussion

Fig. 1 schematically shows the structure of the FSS. The new gel electrolyte was prepared by dissolving PVA in water, followed by addition of H_2SO_4 and PySH. An aligned CNT/MC hybrid fiber had been prepared by coating MC onto aligned CNT sheets drawn from spinnable multi-walled CNT arrays (Fig. S1 and S2†), followed by rolling into a fiber. Fig. 2a and b compare scanning electron microscopy (SEM) images of a CNT fiber before and after coating MC particles. The bare CNT fiber displays a diameter of ~36 μm, while the CNT/MC hybrid fibers show increased diameters after incorporation of MC particles with sizes of hundreds of nanometers to several micrometers (Fig. S3†). The diameters of CNT/MC hybrid fibers are appropriately 53, 81, 110, and 134 μm with the increasing MC weight percentages of 32%, 53%, 68% and 86%, respectively (Fig. S4 and S5†). 68% wt% of MC has been mainly used if not specified.

Table 1 Comparison of FSSs with different gel electrolytes

Electrolyte	C_L (mF cm^{-1})	C_A (mF cm^{-2})	C_V (mF cm^{-3})
PVA–H_2SO4	2.01 ± 0.12	58.08 ± 3.47	21.12 ± 1.26
PVA–H_2SO4–PySH	17.51 ± 1.32	507.02 ± 38.22	184.37 ± 13.90

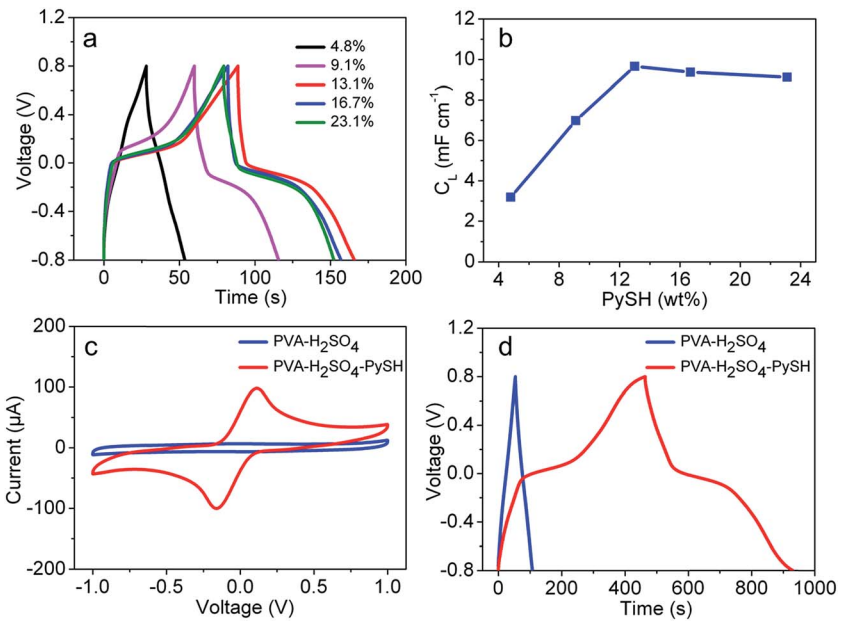

Fig. 3 (a) Galvanostatic charge/discharge curves of FSSs based on the PVA–H_2SO_4–PySH gel electrolyte with different weight percentages of 2-mercaptopyridine (PySH) at a current density of 2.90 mA cm^{-2}. (b) Length specific capacitances (C_L) of FSSs with different weight percentages of PySH at a current density of 2.90 mA cm^{-2}. (c) CV curves for PVA–H_2SO_4 and PVA–H_2SO_4–PySH (PySH weight percentage of 13.1%) gel electrolytes at a scan rate of 5 mV s^{-1}. (d) Galvanostatic charge/discharge curves of PVA–H_2SO_4 and PVA–H_2SO_4–PySH (PySH weight percentage of 13.1%) gel electrolytes at a current density of 0.87 mA cm^{-2}.

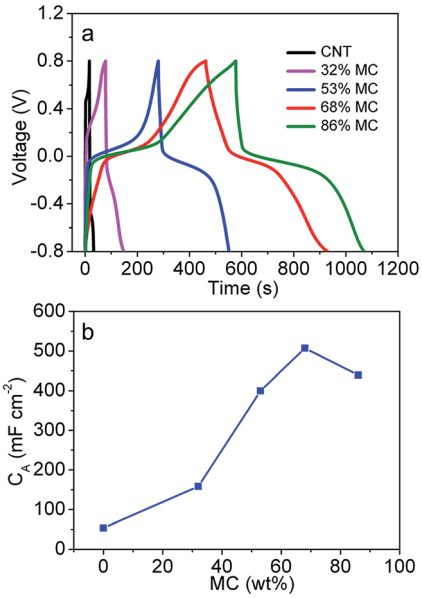

Fig. 4 (a) Galvanostatic charge/discharge curves of FSSs with different MC weight percentages at a current of 30 μA. (b) Area specific capacitances (C_A) of FSSs with different MC weight percentages at a current of 30 μA.

Fig. 2c and d further show that the MC particles are infiltrated among aligned CNTs. Due to a highly ordered and uniform mesoporous structure (Fig. S6†), the MC has a high specific surface area of 1067 $m^2 g^{-1}$ that is important for the use of the redox-active gel electrolyte in energy storage (Fig. S7†). The introduction of MC provides the hybrid fiber with a surface area of 923 $m^2 g^{-1}$, much higher than 160 $m^2 g^{-1}$ for the bare CNT fiber (Fig. S8 and S9†).

The PVA–H_2SO_4–PySH gel electrolyte was coated onto the surface of the hybrid fiber, and two coated fibers were then twisted to produce the FSS. Fig. 3a compares galvanostatic charge/discharge curves of the FSSs using PVA–H_2SO_4–PySH gel electrolytes with increasing PySH weight percentages under the same other conditions. Below 13.1%, the redox shuttle cannot be effectively realized; beyond the point, the specific capacitances are slightly decreased with the increasing PySH weight percentage (Fig. 3b). The highest specific capacitance occurs at 13.1%.

Cyclic voltammetry (CV) was also used to study the electrochemical properties of FSSs based on this novel electrolyte. Fig. 3c compares CV curves of the FSSs derived from PVA–H_2SO_4 and PVA–H_2SO_4–PySH gel electrolytes under the same conditions. Obviously, without PySH, the CV curve shows a typical

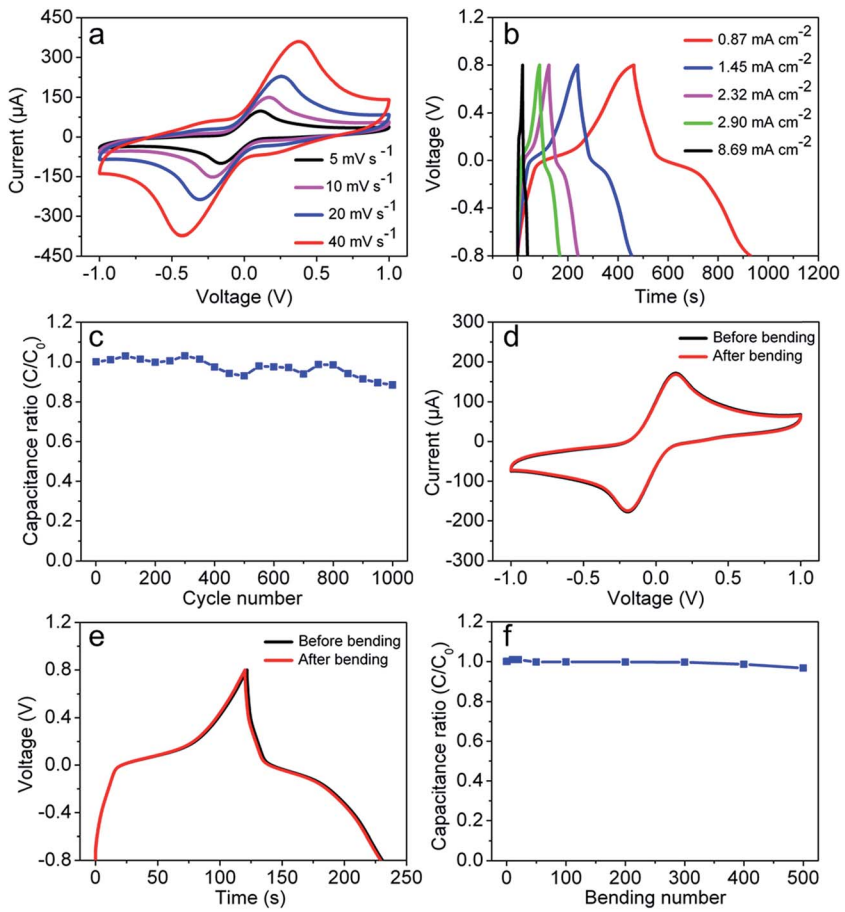

Fig. 5 Electrochemical performances of the FSS with the PVA–H_2SO_4–PySH (PySH weight percentage of 13.1%) gel electrolyte. (a) CV curves at different scan rates. (b) Galvanostatic charge/discharge curves at different current densities. (c) Dependence of capacitance ratio on the cycle number. (d) CV curves before and after bending at a scan rate of 10 mV s^{-1}. (e) Galvanostatic charge/discharge curves before and after bending at a current density of 2.32 mA cm^{-2}. (f) Dependence of specific capacitance on the bending number.

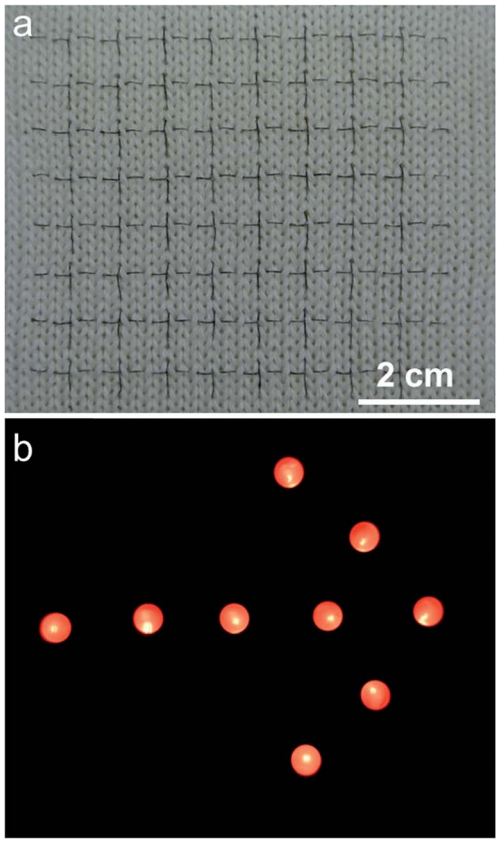

Fig. 6 (a) FSSs being woven into a fabric. (b) Three FSSs being connected in series to lighten up nine red light emission diodes.

rectangular shape, indicating an electric double-layer capacitance. In contrast, a much higher current and a pair of broad and symmetric redox peaks are observed for the new electrolyte with the PySH due to the redox reaction of PySH at the electrolyte/electrode interface. Therefore, a higher specific capacitance may be expected for the resulting FSS.

Fig. 3d further compares galvanostatic charge/discharge curves of the FSSs without and with the PySH. In the new electrolyte with PySH, a voltage plateau between 0 and 0.2 V agrees with the CV result. The curve is nearly symmetric during charge and discharge processes, indicating a high reversibility. In addition, the PVA–H_2SO_4–PySH gel electrolyte based supercapacitor shows a much longer discharge time. As a result, the specific capacitance is nine times that of the PVA–H_2SO_4 gel electrolyte without PySH. The area specific capacitance of 507.02 mF cm^{-2} is also much higher than the previous FSSs.[16,21] The length specific capacitance (C_L) and volume specific capacitance (C_V) are also summarized in Table 1.

The MC content was found to largely affect the electrochemical performance of the resulting FSS. Fig. 4a compares the galvanostatic charge/discharge curves of the FSSs with increasing MC weight percentages under the same other conditions. When the MC weight percentage is lower than 32%, the plateau is weak due to less redox-active reactions for a less content of the MC particle at the electrode/electrolyte interface. The capacitances are increased with the increasing MC weight percentage below 68% and then slightly increased beyond this point. Fig. 4b further shows that the maximal area specific capacitance occurs at the MC weight percentage of 68%.

The FSS based on the PVA–H_2SO_4–PySH gel electrolyte with the PySH weight percentage of 13.1% had been further carefully investigated. Fig. 5a shows CV curves with increasing scan rates, and the curve shapes have been well maintained. The high electrochemical stability is also verified by the symmetric galvanostatic charge/discharge curves (Fig. 5b). In addition, the specific capacitance of the FSS can be maintained by over 88% after 1000 charge/discharge cycles (Fig. 5c).

As expected, the FSS is flexible and investigated during bending. Both CV and galvanostatic charge/discharge curves are overlapped well before and after bending (Fig. 5d and e). The flexibility of FSSs was further quantitatively studied by tracing the specific capacitances during bending. They can be maintained by 97% after bending for 500 cycles (Fig. 5f). The flexible FSSs can be easily woven into the fabric (Fig. 6a). They were assembled in series or parallel to tune the output voltage or current, respectively. For instance, Fig. S10† compares galvanostatic charge/discharge curves of single and three FSSs in series at the same charge/discharge current. The potential window is increased from 0.8 to 2.4 V for the connected three FSSs. These FSSs can efficiently power nine red light emission diodes (Fig. 6b).

Conclusion

In summary, we have presented a general and effective strategy to fabricate novel FSSs with a high specific capacitance of 507.02 mF cm^{-2} by developing and incorporating a redox-active gel electrolyte. Therefore, the proposed advantages of FSSs that may be woven into textiles or integrated into other structures to satisfy the wearable facilities, portable devices and various miniaturized products can be effectively achieved. This strategy may be also extended to the other flexible electrochemical energy storage devices aiming at a high capability.

Acknowledgements

This work was supported by MOST (2011CB932503), NSFC (21225417), STCSM (12nm0503200), the Fok Ying Tong Education Foundation, the Program for Special Appointments of Professors at Shanghai Institutions of Higher Learning, and the Program for Outstanding Young Scholars from the Organization Department of the CPC Central Committee.

References

1 W. Zeng, L. Shu, Q. Li, S. Chen, F. Wang and X. M. Tao, *Adv. Mater.*, 2014, **26**, 5310.
2 Y. Fu, X. Cai, H. Wu, Z. Lv, S. Hou, M. Peng, X. Yu and D. Zou, *Adv. Mater.*, 2012, **24**, 5713.
3 J. Bae, M. K. Song, Y. J. Park, J. M. Kim, M. Liu and Z. L. Wang, *Angew. Chem., Int. Ed.*, 2011, **50**, 1683.

4 A. B. Dalton, S. Collins, E. Munoz, J. M. Razal, V. H. Ebron, J. P. Ferraris, J. N. Coleman, B. G. Kim and R. H. Baughman, *Nature*, 2003, **423**, 703.
5 P. Xu, T. Gu, Z. Cao, B. Wei, J. Yu, F. Li, J. H. Byun, W. Lu, Q. Li and T. W. Chou, *Adv. Energy Mater.*, 2014, **4**, 1300759.
6 Y. Meng, Y. Zhao, C. Hu, H. Cheng, Y. Hu, Z. Zhang, G. Shi and L. Qu, *Adv. Mater.*, 2013, **25**, 2326.
7 T. Huang, B. Zheng, L. Kou, K. Gopalsamy, Z. Xu, C. Gao, Y. Meng and Z. Wei, *RSC Adv.*, 2013, **3**, 23957.
8 Y. Li, K. Sheng, W. Yuan and G. Shi, *Chem. Commun.*, 2013, **49**, 291.
9 D. Yu, K. Goh, H. Wang, L. Wei, W. Jiang, Q. Zhang, L. Dai and Y. Chen, *Nat. Nanotechnol.*, 2014, **9**, 555.
10 N. Liu, W. Ma, J. Tao, X. Zhang, J. Su, L. Li, C. Yang, Y. Gao, D. Golberg and Y. Bando, *Adv. Mater.*, 2013, **25**, 4925.
11 G. Sun, J. Liu, X. Zhang, X. Wang, H. Li, Y. Yu, W. Huang, H. Zhang and P. Chen, *Angew. Chem., Int. Ed.*, 2014, **53**, 12576.
12 L. Kou, T. Huang, B. Zheng, Y. Han, X. Zhao, K. Gopalsamy, H. Sun and C. Gao, *Nat. Commun.*, 2014, **5**, 3754.
13 J. Ren, W. Bai, G. Guan, Y. Zhang and H. Peng, *Adv. Mater.*, 2013, **25**, 5965.
14 X. Wang, B. Liu, R. Liu, Q. Wang, X. Hou, D. Chen, R. Wang and G. Shen, *Angew. Chem., Int. Ed.*, 2014, **53**, 1849.
15 B. Zheng, T. Huang, L. Kou, X. Zhao, K. Gopalsamy and C. Gao, *J. Mater. Chem. A*, 2014, **2**, 9736.
16 X. Chen, L. Qiu, J. Ren, G. Guan, H. Lin, Z. Zhang, P. Chen, Y. Wang and H. Peng, *Adv. Mater.*, 2013, **25**, 6436.
17 V. T. Le, H. Kim, A. Ghosh, J. Kim, J. Chang, Q. A. Vu, D. T. Pham, J.-H. Lee, S.-W. Kim and Y. H. Lee, *ACS Nano*, 2013, **7**, 5940.
18 B. Liu, D. Tan, X. Wang, D. Chen and G. Shen, *Small*, 2013, **9**, 1998.
19 C. Choi, J. A. Lee, A. Y. Choi, Y. T. Kim, X. Lepró, M. D. Lima, R. H. Baughman and S. J. Kim, *Adv. Mater.*, 2014, **26**, 2059.
20 X. Xiao, T. Li, P. Yang, Y. Gao, H. Jin, W. Ni, W. Zhan, X. Zhang, Y. Cao and J. Zhong, *ACS Nano*, 2012, **6**, 9200.
21 J. Ren, L. Li, C. Chen, X. Chen, Z. Cai, L. Qiu, Y. Wang, X. Zhu and H. Peng, *Adv. Mater.*, 2013, **25**, 1155.
22 F. Su, X. Lv and M. Miao, *Small*, 2014, **11**, 854.
23 X. Ding, Y. Zhao, C. Hu, Y. Hu, Z. Dong, N. Chen, Z. Zhang and L. Qu, *J. Mater. Chem. A*, 2014, **2**, 12355.
24 K. Wang, Q. Meng, Y. Zhang, Z. Wei and M. Miao, *Adv. Mater.*, 2013, **25**, 1494.
25 J. A. Lee, M. K. Shin, S. H. Kim, H. U. Cho, G. M. Spinks, G. G. Wallace, M. D. Lima, X. Lepró, M. E. Kozlov, R. H. Baughman and S. J. Kim, *Nat. Commun.*, 2013, **4**, 1970.
26 S. Pan, Z. Yang, H. Li, L. Qiu, H. Sun and H. Peng, *J. Am. Chem. Soc.*, 2013, **135**, 10622.